



Study of the electrochemical deposition of Sn–Ag–Cu alloy by cyclic voltammetry and chronoamperometry

Jinqiu Zhang, Maozhong An*, Limin Chang

School of Chemical Engineering and Technology, Harbin Institute of Technology, Harbin, China

ARTICLE INFO

Article history:

Received 11 October 2008

Received in revised form

10 November 2008

Accepted 10 November 2008

Available online 19 November 2008

Keywords:

Electrodeposit

Cyclic voltammetry

Chronoamperometry

Sn–Ag–Cu alloy

Nucleus growth mechanism

ABSTRACT

The electrochemical deposition of Sn–Ag–Cu alloy from weakly acidic baths onto glassy carbon electrodes (GCE) was studied by cyclic voltammetry (CV) and chronoamperometry (CA). The properties of the electrodeposits were characterized by scanning electron microscopy (SEM), energy-dispersive spectrometry (EDS) and X-ray diffraction (XRD). Test results indicate that the two cathodic peaks in the CV curves, at -0.6 V and -0.85 V during the forward scan towards the negative potentials, correspond to the irreversible deposition of a solid solution of tin, silver and copper. The underpotential deposition (UPD) of Sn occurs at -0.6 V during the cathodic period and the amount of Ag and Cu in the Sn–Ag–Cu alloy decreases with increasingly negative cathodic potentials. During the forward scan, towards the positive potentials used in CV testing, cathodic peaks at -0.85 V appear in the CV curves for baths containing mixtures of tin salts and triethanolamine (TEA). This corresponds to a reduction of transient complex ions $[\text{Sn}(\text{TEA})_x]^{2+}$ on the surface of the cathode. Furthermore, the formation and reduction of $[\text{Sn}(\text{TEA})_x]^{2+}$ is a diffusion controlled process. On the surface of the GCE, the actual nucleus growth mechanism of the Sn–Ag–Cu alloy is represented by the progressive nucleation model.

© 2008 Elsevier Ltd. All rights reserved.

1. Introduction

Tin–lead alloys are the most widely used solder coatings in traditional electronic packaging. However, the acute toxicity of lead has spurred legislation banning its use in electronic products. Near eutectic Sn–Ag–Cu alloys [1–8] are now being developed as promising lead-free solder coatings. These alloys demonstrate superior mechanical properties and solderability [9,10]. We electrodeposited bright, compact and smooth Sn–Ag–Cu alloy coatings. These coatings contain 88–95 wt.% Sn, 5–10 wt.% Ag and 0.5–2 wt.% Cu. They were produced from weakly acidic baths that contained three main salts, three complexing agents, one main brightener and one antioxidant [11]. In this kind of complicated electrolyte, the properties and quality of the alloy coatings are directly determined by mechanism of electrocrystallization. Therefore, it is of great significance to study the electrochemical deposition of Sn–Ag–Cu alloys to improve the properties and quality of these coatings.

To the best of our knowledge, not much work has been done on the electroplating mechanism of Sn–Ag–Cu alloy coatings. The polarization curves and surface morphology show that the elec-

trodeposition of a Sn–Ag–Cu alloy coating from an alkaline bath represents a normal co-deposition [3]. The cyclic voltammograms of a Sn–Ag–Cu electroplating bath that contained methanesulphonic acid (MSA) were measured to analyze the effect of iso-octyl phenoxy polyethoxy ethanol (OPPE) and thiourea on the co-deposition [5].

CV and CA techniques were used to investigate the electrodeposition behavior, rate controlling step, and the nucleus growth mechanism of Sn–Ag–Cu alloy electrodeposited from a weakly acidic bath.

2. Experimental

2.1. Compositions of bath

The electroplating bath for bright Sn–Ag–Cu alloy contained 0.20 mol L^{-1} $\text{Sn}(\text{CH}_3\text{SO}_3)_2$, 4.5 mmol L^{-1} AgI, 1.5 mmol L^{-1} $\text{Cu}(\text{CH}_3\text{SO}_3)_2$, 0.60 mol L^{-1} $\text{K}_4\text{P}_2\text{O}_7$, 1.35 mol L^{-1} KI, 0.225 mol L^{-1} TEA, 6.4 mmol L^{-1} heliotropin (HT) and 9 mmol L^{-1} hydroquinone. Among these compositions, $\text{Sn}(\text{CH}_3\text{SO}_3)_2$, AgI and $\text{Cu}(\text{CH}_3\text{SO}_3)_2$ are the main salts, $\text{K}_4\text{P}_2\text{O}_7$, KI and TEA are complexing agents, HT is a main brightener and hydroquinone is an antioxidant [11]. The pH of the bath was adjusted to 5.5 by MSA. The bath undergoing investigation was modified according to the different experimental requirements. The bath components were modified, while pH was kept constant.

* Corresponding author. Tel.: +86 45186413721; fax: +86 45186415527.

E-mail address: mzan@hit.edu.cn (M. An).

2.2. Electrochemical evaluation

CV and CA experiments were carried out in a three-electrode glass cell on a CHI630B electrochemical workstation. A saturated calomel electrode (SCE) was used as the reference electrode and platinum foil (99.99%, 2 cm²) was used as the counter-electrode. The working electrode was a GCE with a working surface of 7.1 mm² ($\varnothing = 3$ mm). A Luggin capillary tip was set 2 mm from the surface of the working electrode. The bath temperature was maintained at 20 ± 1 °C by thermostat control. CV curves were recorded at a scanning rate of 100 mV s⁻¹.

2.3. Properties of Sn–Ag–Cu alloy electrodeposits

The deposition of Sn–Ag–Cu alloy was carried out potentiostatically on a HDV-07 instrument. The working electrode was a Fe/Ni foil with a working surface area of 750 mm² (25 mm × 30 mm). The electrodeposition time varied from 30 min to 120 min. The deposition charge that was calculated from the current-time curves was 2200 C dm⁻². The surface morphologies of the Sn–Ag–Cu alloy electrodeposits were analyzed using a S-570 SEM. The chemical composition of the electrodeposits was determined by EDS in the S-570 SEM. The crystal structure of the deposit was examined using a D/max-3C XRD with Cu K α radiation.

3. Results and discussion

3.1. Analysis of cyclic voltammograms

Transient cyclic voltammograms are an efficacious method used to study the reactions on the working electrode surface. The cathode electrode reactions in the electrodeposition process of Sn–Ag–Cu ternary alloy are complicated. Therefore, it is necessary to study the CV behaviors of single metals and binary alloys before the CV curves of the Sn–Ag–Cu alloy can be studied.

As shown in Fig. 1, during the forward scan towards the negative potentials, a very small cathodic current is observed. It is attributed to the reduction of impurities or oxygen dissolved in the bath. The onset of Sn deposition is at about -1.26 V. There is a sharp increase in the cathodic current, followed by the current looping as the direction of the sweep is reversed. The appearance of this type of hysteresis loop (ABC) is a characteristic feature of

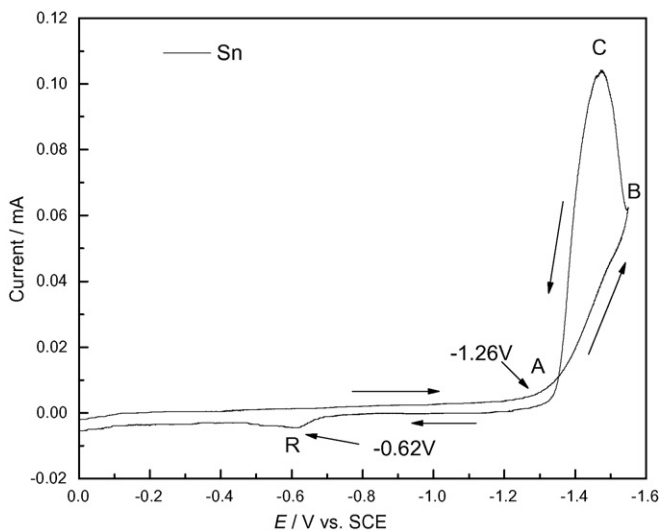


Fig. 1. CV curves of tin electrodeposited from a weakly acidic bath containing 0.20 mol L⁻¹ Sn(CH₃SO₃)₂, 0.60 mol L⁻¹ K₄P₂O₇, 1.35 mol L⁻¹ KI, 0.225 mol L⁻¹ TEA, 6.4 mmol L⁻¹ HT and 9 mmol L⁻¹ hydroquinone at a scan rate of 100 mV s⁻¹.

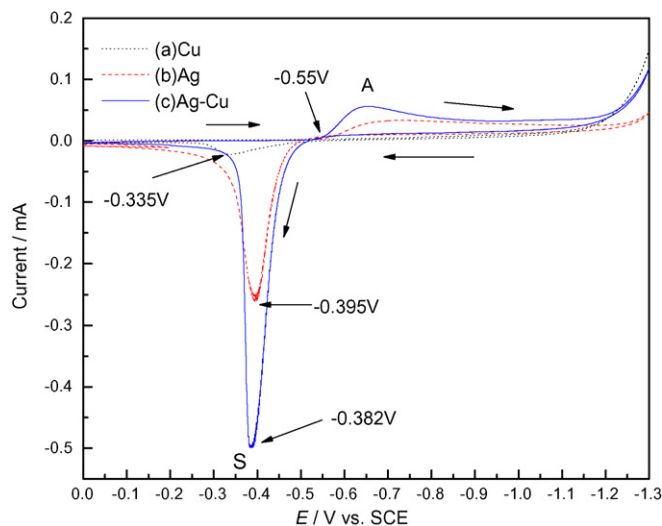


Fig. 2. CV curves of Cu, Ag and Ag–Cu electrodeposited from weakly acidic baths containing 0.60 mol L⁻¹ K₄P₂O₇, 1.35 mol L⁻¹ KI, 0.225 mol L⁻¹ TEA, 6.4 mmol L⁻¹ HT, 9 mmol L⁻¹ hydroquinone and (a) 1.5 mmol L⁻¹ Cu(CH₃SO₃)₂, (b) 4.5 mmol L⁻¹ AgI, (c) 4.5 mmol L⁻¹ AgI and 1.5 mmol L⁻¹ Cu(CH₃SO₃)₂ at a scan rate of 100 mV s⁻¹.

a nucleation and growth process [12]. An anodic peak 'R' appears at -0.62 V during the anodic period. This peak corresponds to the dissolution of tin. The area of the cathodic peak is larger than that of the anodic peak because most of the cathodic current generates hydrogen. The exclusive electrodeposition of Sn is difficult in the bath without other metal ions.

As shown in Fig. 2a and b, the anodic peaks at -0.335 V and -0.395 V correspond to the dissolution of copper and silver, respectively. In a simple salt bath, the anodic peak position of Ag should be more positive than that of Cu. However, the anodic peak position of Cu in Fig. 2a is more positive than that of Ag in Fig. 2b. This can be attributed to the large quantity of KI existing in the bath. KI is used as a complexing agent for Ag⁺. The anodic peak area in Fig. 2a is the smallest because the concentration of copper ions is the lowest among metal ions in the bath. As shown in Fig. 2c, an anodic peak appears at -0.382 V during the anodic period. The area of the anodic peak is the largest. This means that the anodic peak is the dissolution peak of a solid solution of silver and copper.

As shown in Fig. 3a–c, scanning towards the positive potentials result in anodic peaks at -0.638 V, -0.634 V and -0.627 V, respectively. These anodic peaks have a potential value similar to that of tin (Fig. 1); they also correspond to the dissolution of tin. By adding tin salt to the bath, the potentials of the peaks at about -0.4 V in Fig. 3a–c are different from those of the curves shown in Fig. 2a–c. The anodic currents of the peaks at -0.4 V in Fig. 3a–c are bigger than the corresponding curves in Fig. 2a–c. This means that these anodic peaks in Fig. 3 correspond to the dissolution of a solid solution containing tin. As shown in Fig. 3c, two cathodic peaks at -0.6 V and -0.85 V form during the cathodic period. In order to determine the relationships between the cathodic and anodic peaks in Fig. 3c, we investigated the effect of the scan reversal potential on anodic peaks of the CV curves. As shown in Fig. 4, cathodic peak 'A' corresponds to the anodic peak 'S'. The Sn–Ag–Cu alloy coating, electrodeposited potentiostatically at -0.6 V, is composed of 60.1 at% Sn, 11.2 at% Ag and 28.7 at% Cu. This means that peak 'A' is the co-deposit peak of the Sn–Ag–Cu alloy, and peak 'S' is the dissolution peak of the solid solution of tin, silver and copper. The exclusive electrodeposition of Sn is difficult (Fig. 1), therefore, the reduction of Sn²⁺ ions at -0.6 V in the weakly acidic bath can be modeled as underpotential deposition (UPD) of Sn on Ag and Cu atoms [13]. The composition of the small round grains in region 'A'

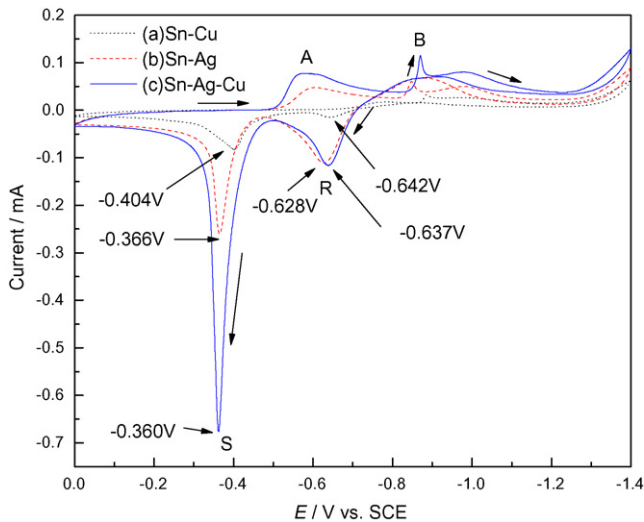


Fig. 3. CV curves of Sn–Cu, Sn–Ag and Sn–Ag–Cu electrodeposited from weakly acidic baths containing $0.20 \text{ mol L}^{-1} \text{ Sn}(\text{CH}_3\text{SO}_3)_2$, $0.60 \text{ mol L}^{-1} \text{ K}_4\text{P}_2\text{O}_7$, $1.35 \text{ mol L}^{-1} \text{ KI}$, $0.225 \text{ mol L}^{-1} \text{ TEA}$, $6.4 \text{ mmol L}^{-1} \text{ HT}$, 9 mmol L^{-1} hydroquinone and (a) $1.5 \text{ mmol L}^{-1} \text{ Cu}(\text{CH}_3\text{SO}_3)_2$, (b) $4.5 \text{ mmol L}^{-1} \text{ AgI}$, (c) $4.5 \text{ mmol L}^{-1} \text{ AgI}$ and $1.5 \text{ mmol L}^{-1} \text{ Cu}(\text{CH}_3\text{SO}_3)_2$ at a scan rate of 100 mV s^{-1} .

of Fig. 5 is 24.9 at% Sn, 29.3 at% Ag and 45.8 at% Cu; this confirms the above presumption.

As shown in Fig. 6a, the scan reversal potential is -0.90 V . Peak 'K' appears at -0.44 V , which is near peak 'S', during the anodic period. When the scan reversal potential is -0.95 V , there is superposition between peak 'S' and peak 'K' (Fig. 6b). When the scan reversal potential is -1.1 V , peak 'K' disappears as shown in Fig. 6c. In addition, as shown in Fig. 7, the coexistence of peak 'K' and peak 'S' is observed by testing other baths of electrodeposited Sn–Ag and Sn–Cu alloys when the scan reversal potential is -0.90 V . It is presumed that, peak 'K' is the dissolution peak of some ambiguous intermetallic compound (IMC). When the scan reversal potential is increasingly negative, the dissolution peak of the solid solution covers up the ambiguous IMC. It can be seen that the anodic current of peak 'S' in Fig. 6a is larger than the same 'S' peak in Fig. 4. Therefore, peak 'B' is mainly related to peaks 'S' and 'K'. Therefore, peak 'B'

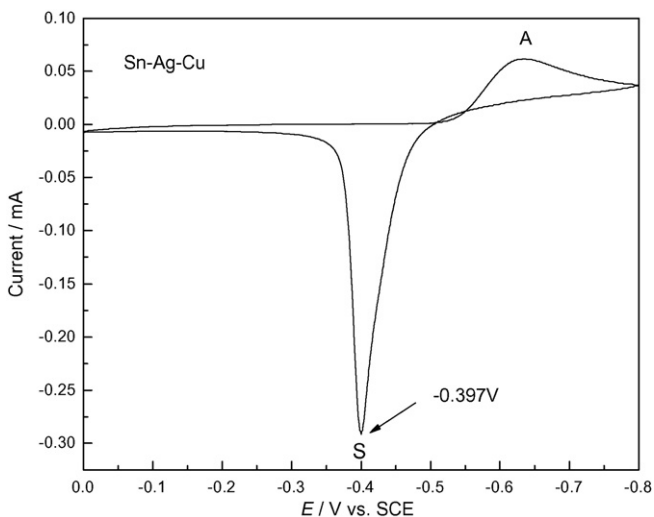


Fig. 4. CV curves of Sn–Ag–Cu alloy electrodeposited in a weakly acidic bath containing $0.20 \text{ mol L}^{-1} \text{ Sn}(\text{CH}_3\text{SO}_3)_2$, $4.5 \text{ mmol L}^{-1} \text{ AgI}$, $1.5 \text{ mmol L}^{-1} \text{ Cu}(\text{CH}_3\text{SO}_3)_2$, $0.60 \text{ mol L}^{-1} \text{ K}_4\text{P}_2\text{O}_7$, $1.35 \text{ mol L}^{-1} \text{ KI}$, $0.225 \text{ mol L}^{-1} \text{ TEA}$, $6.4 \text{ mmol L}^{-1} \text{ HT}$ and 9 mmol L^{-1} hydroquinone in scan potential range of 0 V to -0.8 V at a scan rate of 100 mV s^{-1} .

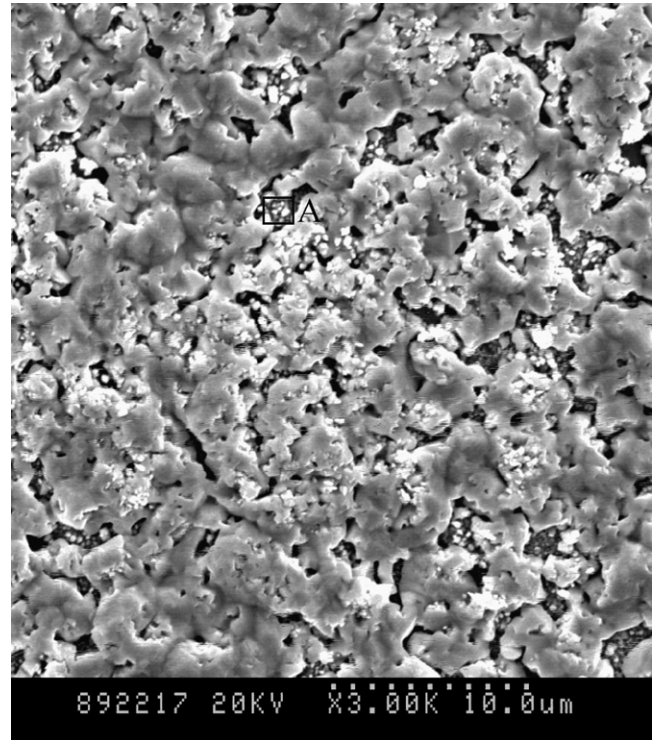


Fig. 5. SEM image of a Sn–Ag–Cu alloy coating electrodeposited potentiostatically at -0.6 V from a weakly acidic bath containing $0.20 \text{ mol L}^{-1} \text{ Sn}(\text{CH}_3\text{SO}_3)_2$, $4.5 \text{ mmol L}^{-1} \text{ AgI}$, $1.5 \text{ mmol L}^{-1} \text{ Cu}(\text{CH}_3\text{SO}_3)_2$, $0.60 \text{ mol L}^{-1} \text{ K}_4\text{P}_2\text{O}_7$, $1.35 \text{ mol L}^{-1} \text{ KI}$, $0.225 \text{ mol L}^{-1} \text{ TEA}$, $6.4 \text{ mmol L}^{-1} \text{ HT}$ and 9 mmol L^{-1} hydroquinone.

is the co-deposit peak for large quantities of Sn–Ag–Cu solid solution and small quantities of ambiguous IMC. The Sn–Ag–Cu alloy coating, electrodeposited potentiostatically at -0.85 V , is composed of 78.9 at% Sn, 14.8 at% Ag and 6.3 at% Cu. The stone-like grains in region 'A' of Fig. 8 are composed of 72.1 at% Sn, 17.5 at% Ag and 10.4 at% Cu. The higher contents of Ag and Cu in region 'A' can be attributed to the electrodeposition of IMC.

Fig. 3c shows a straight increase in the cathodic current during the potential change from -1.25 V to -1.4 V . This corresponds to the co-deposition of the Sn–Ag–Cu alloy. The Sn–Ag–Cu alloy coating, electrodeposited potentiostatically at -1.4 V , is bright and smooth, with a fine morphology (Fig. 9). The Ag and Cu contents in the coating are 8.9 at% and 4.8 at%, respectively. These values are lower than those from the coating electrodeposited potentiostatically at -0.6 V and -0.85 V . The Ag and Cu content within the Sn–Ag–Cu alloy decreases, as the cathodic potential is increasingly negative. As shown in Fig. 10, the diffraction peaks in the Sn–Ag–Cu alloy coating can be attributed to the β -Sn, Ag_3Sn and Cu_6Sn_5 phases. Peak 'R' in Fig. 3c is clearly the dissolution peak of Sn, and peak 'S' in Fig. 3c is clearly the dissolution peak of a solid solution containing little IMC. Different compositions of solid solution and IMC, under various conditions, will shift the potential position of the 'S' peak.

As shown in Fig. 6c, a strong cathodic peak 'Q' appears at about -0.85 V during the forward scan towards the positive potentials. The current of peak 'Q' is higher than that of peak 'B'. However, the current of peak 'Q' decreases as the scan reversal potential becomes more negative (Fig. 3c). This means that peak 'Q' is a reductive peak of some transient complex ions. As shown in Fig. 11, the current values associated with peaks 'Q' and 'R' decrease as the number of scans increase. This implies some sort of interrelation between peaks 'Q' and 'R'. As shown in Fig. 2, peak 'Q' does not appear in the CV curves for the baths without Sn^{2+} ions. As shown in Fig. 12, peak 'Q' also does not appear in the CV curves for the bath without TEA. It can be seen from Figs. 2, 3 and 12, that peak 'Q' only

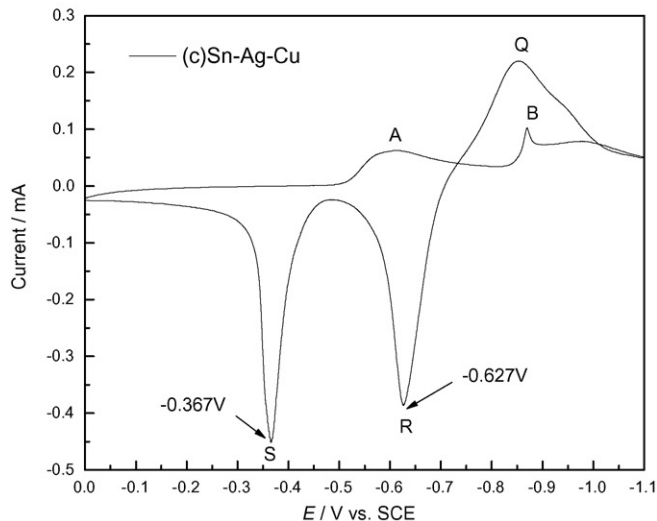
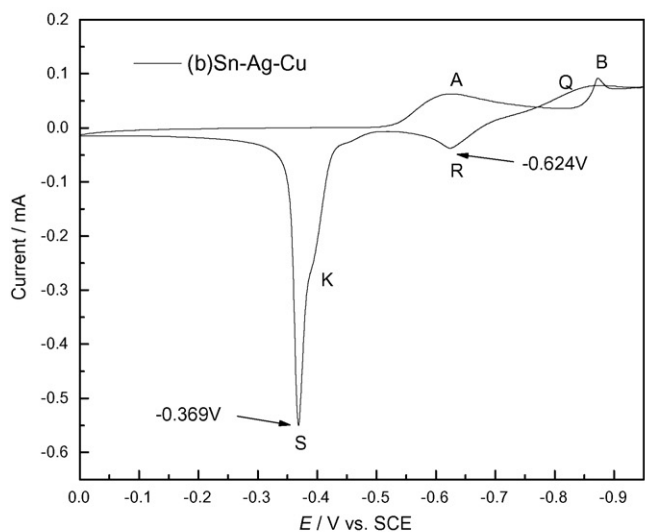
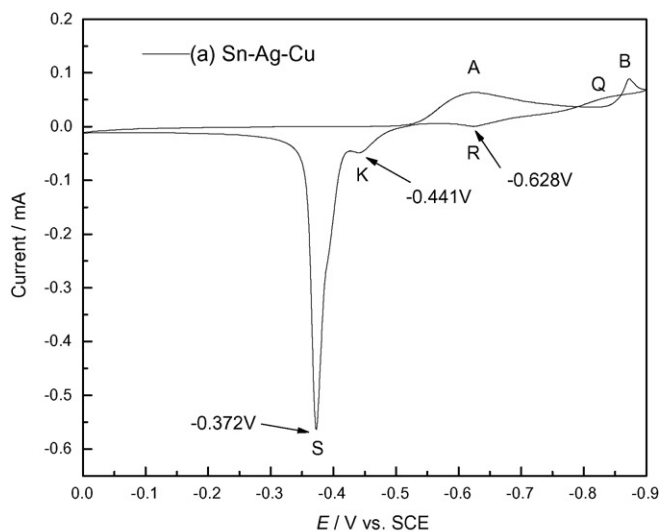


Fig. 6. CV curves of Sn–Ag–Cu alloy electrodeposited from a weakly acidic bath containing $0.20 \text{ mol L}^{-1} \text{ Sn}(\text{CH}_3\text{SO}_3)_2$, $4.5 \text{ mmol L}^{-1} \text{ AgI}$, $1.5 \text{ mmol L}^{-1} \text{ Cu}(\text{CH}_3\text{SO}_3)_2$, $0.60 \text{ mol L}^{-1} \text{ K}_4\text{P}_2\text{O}_7$, $1.35 \text{ mol L}^{-1} \text{ KI}$, $0.225 \text{ mol L}^{-1} \text{ TEA}$, $6.4 \text{ mmol L}^{-1} \text{ HT}$ and $9 \text{ mmol L}^{-1} \text{ hydroquinone}$ in different scan potential ranges: (a) 0 V to -0.9 V , (b) 0 V to -0.95 V and (c) 0 V to -1.1 V at a scan rate of 100 mV s^{-1} .

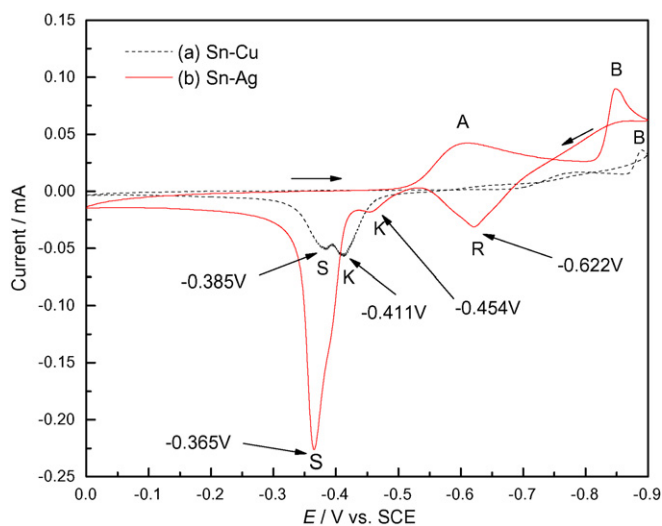


Fig. 7. CV curves of Sn–Cu and Sn–Ag alloys electrodeposited from weakly acidic baths containing $0.20 \text{ mol L}^{-1} \text{ Sn}(\text{CH}_3\text{SO}_3)_2$, $0.60 \text{ mol L}^{-1} \text{ K}_4\text{P}_2\text{O}_7$, $1.35 \text{ mol L}^{-1} \text{ KI}$, $0.225 \text{ mol L}^{-1} \text{ TEA}$, $6.4 \text{ mmol L}^{-1} \text{ HT}$, $9 \text{ mmol L}^{-1} \text{ hydroquinone}$ and (a) $1.5 \text{ mmol L}^{-1} \text{ Cu}(\text{CH}_3\text{SO}_3)_2$, (b) $4.5 \text{ mmol L}^{-1} \text{ AgI}$ at a scan rate of 100 mV s^{-1} .

appears in the CV curves for the bath containing a mixture of tin salts and TEA. This confirmed that the transient complex ions correspond to tin and TEA. In the bath, TEA is used as a complexing agent for Cu^{2+} , and TEA acts as an assistant brightener, and can decrease cathodic polarization [11]. Considering the complexing effect from TEA, it is presumed that during the cathodic period, tin pyrophosphate complex ions decompose. This is particularly because the potential is more negative and the tin–TEA transient complex ions, expressed as $[\text{Sn}(\text{TEA})_x]^{2+}$, form. Peak ‘Q’ and peak

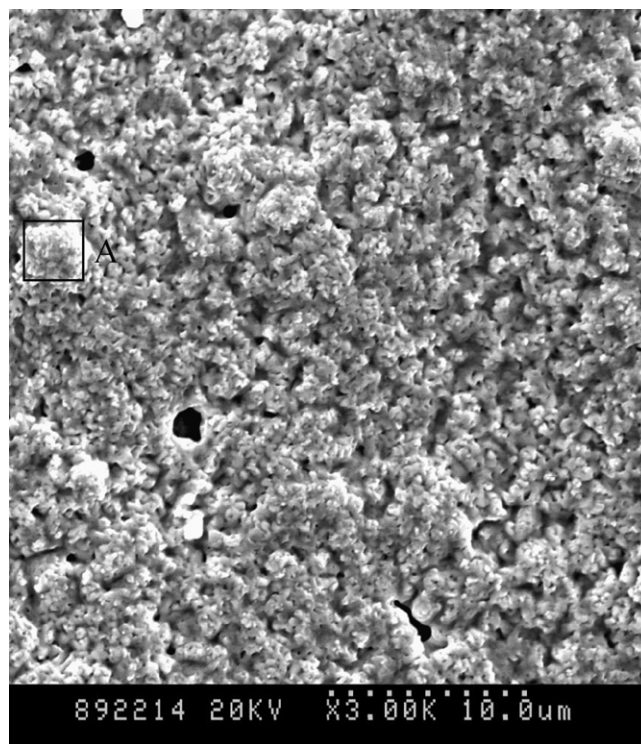


Fig. 8. SEM image of a Sn–Ag–Cu alloy coating electrodeposited potentiostatically at -0.85 V from a weakly acidic bath containing $0.20 \text{ mol L}^{-1} \text{ Sn}(\text{CH}_3\text{SO}_3)_2$, $4.5 \text{ mmol L}^{-1} \text{ AgI}$, $1.5 \text{ mmol L}^{-1} \text{ Cu}(\text{CH}_3\text{SO}_3)_2$, $0.60 \text{ mol L}^{-1} \text{ K}_4\text{P}_2\text{O}_7$, $1.35 \text{ mol L}^{-1} \text{ KI}$, $0.225 \text{ mol L}^{-1} \text{ TEA}$, $6.4 \text{ mmol L}^{-1} \text{ HT}$ and $9 \text{ mmol L}^{-1} \text{ hydroquinone}$.

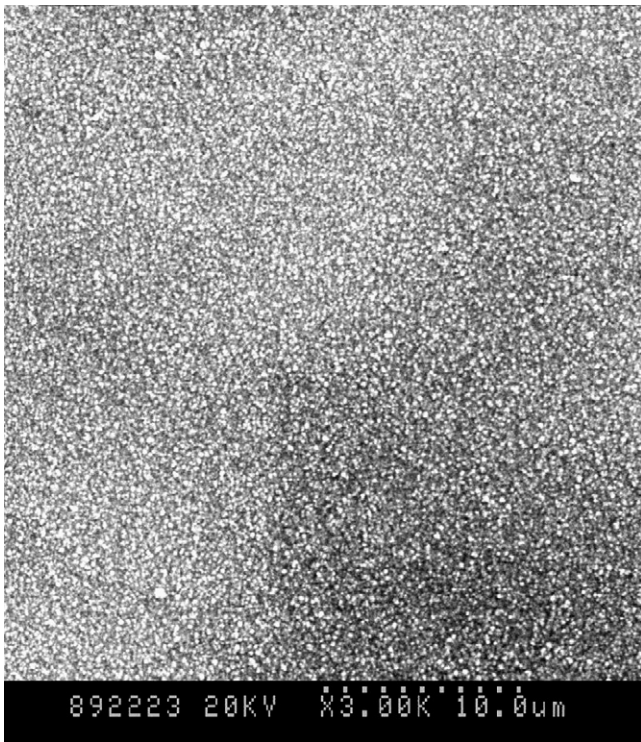


Fig. 9. SEM image of a Sn–Ag–Cu alloy coating electrodeposited potentiostatically at -1.4 V from weakly acidic bath containing $0.20 \text{ mol L}^{-1} \text{ Sn}(\text{CH}_3\text{SO}_3)_2$, $4.5 \text{ mmol L}^{-1} \text{ AgI}$, $1.5 \text{ mmol L}^{-1} \text{ Cu}(\text{CH}_3\text{SO}_3)_2$, $0.60 \text{ mol L}^{-1} \text{ K}_4\text{P}_2\text{O}_7$, $1.35 \text{ mol L}^{-1} \text{ KI}$, $0.225 \text{ mol L}^{-1} \text{ TEA}$, $6.4 \text{ mmol L}^{-1} \text{ HT}$ and 9 mmol L^{-1} hydroquinone.

'R' are strong in Fig. 6c. This corresponds to $[\text{Sn}(\text{TEA})_x]^{2+}$ formation. The scan potential reverses to positive direction at -1.1 V, so there is not enough time for reductive action of $[\text{Sn}(\text{TEA})_x]^{2+}$ ions during cathodic period. The amount of cathodic polarization is reduced by TEA, and the reduction of $[\text{Sn}(\text{TEA})_x]^{2+}$ takes place at a relative positive potential (about -0.85 V) during the anodic period. This results in a strong reductive peak. The current associated with peak 'Q' decreases with the increasing scan times because $[\text{Sn}(\text{TEA})_x]^{2+}$ is not replenished quickly enough after its consumption. Moreover, the formation and reduction of $[\text{Sn}(\text{TEA})_x]^{2+}$ is controlled by diffusion.

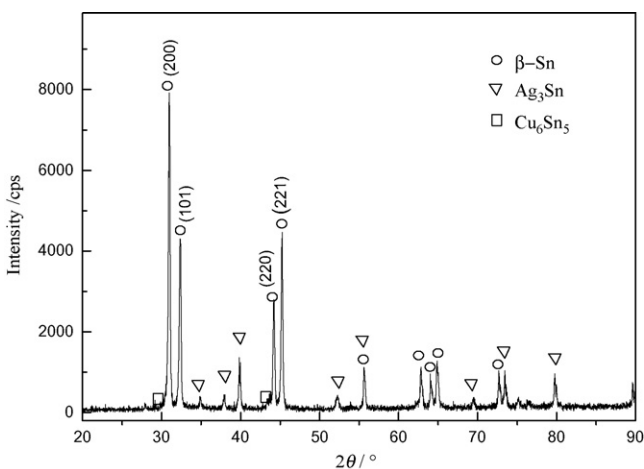


Fig. 10. XRD patterns of a Sn–Ag–Cu alloy coating electrodeposited potentiostatically at -1.4 V from a weakly acidic bath containing $0.20 \text{ mol L}^{-1} \text{ Sn}(\text{CH}_3\text{SO}_3)_2$, $4.5 \text{ mmol L}^{-1} \text{ AgI}$, $1.5 \text{ mmol L}^{-1} \text{ Cu}(\text{CH}_3\text{SO}_3)_2$, $0.60 \text{ mol L}^{-1} \text{ K}_4\text{P}_2\text{O}_7$, $1.35 \text{ mol L}^{-1} \text{ KI}$, $0.225 \text{ mol L}^{-1} \text{ TEA}$, $6.4 \text{ mmol L}^{-1} \text{ HT}$ and 9 mmol L^{-1} hydroquinone.

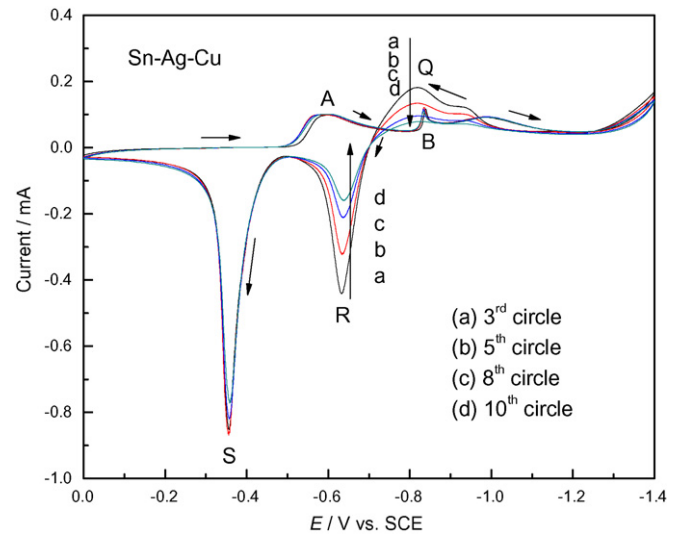


Fig. 11. CV curves of a Sn–Ag–Cu alloy electrodeposited from a weakly acidic bath containing $0.20 \text{ mol L}^{-1} \text{ Sn}(\text{CH}_3\text{SO}_3)_2$, $4.5 \text{ mmol L}^{-1} \text{ AgI}$, $1.5 \text{ mmol L}^{-1} \text{ Cu}(\text{CH}_3\text{SO}_3)_2$, $0.60 \text{ mol L}^{-1} \text{ K}_4\text{P}_2\text{O}_7$, $1.35 \text{ mol L}^{-1} \text{ KI}$, $0.225 \text{ mol L}^{-1} \text{ TEA}$, $6.4 \text{ mmol L}^{-1} \text{ HT}$, 9 mmol L^{-1} hydroquinone at (a) 3rd circle, (b) 5th circle, (c) 8th circle and (d) 10th circle at a scan rate of 100 mV s^{-1} .

3.2. Rate controlling step and nucleus growth mechanism of electrodeposition of Sn–Ag–Cu alloy

In Fig. 13 we see that an increase in the scan rate shifts the reduction peak to a more negative potential; the higher current contribution means that the electrodeposition of Sn–Ag–Cu in a weakly acidic bath is irreversible.

When the electrode reaction is controlled by diffusion processes, the relationship between the peak current intensity and scan rate of CV curves can be expressed as:

$$I_p = 0.4958(nF)^{3/2}(\alpha D\nu)^{1/2}(RT)^{1/2}Ac^* \quad (1)$$

where I_p is the peak current intensity, ν is the potential scan rate, A is the surface area of the working electrode, c^* is the bulk concentration of reducible ions, n is the number of electrons, D is the diffusion coefficient, R is the gas constant, T is the temperature,

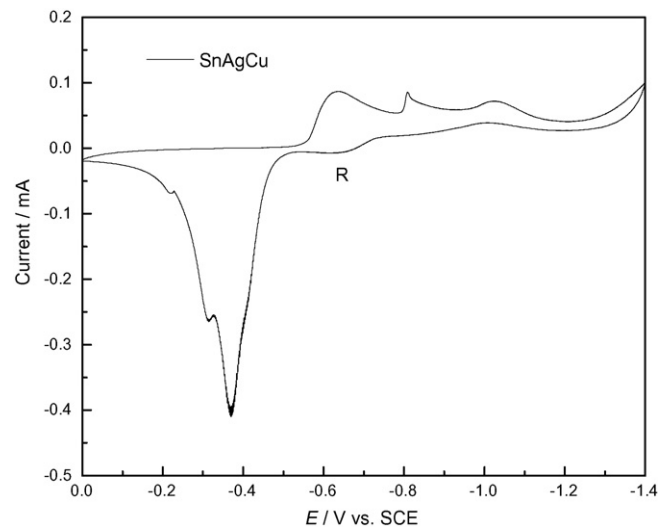


Fig. 12. CV curves of a Sn–Ag–Cu alloy electrodeposited from a weakly acidic bath containing $0.20 \text{ mol L}^{-1} \text{ Sn}(\text{CH}_3\text{SO}_3)_2$, $4.5 \text{ mmol L}^{-1} \text{ AgI}$, $1.5 \text{ mmol L}^{-1} \text{ Cu}(\text{CH}_3\text{SO}_3)_2$, $0.60 \text{ mol L}^{-1} \text{ K}_4\text{P}_2\text{O}_7$, $1.35 \text{ mol L}^{-1} \text{ KI}$, $6.4 \text{ mmol L}^{-1} \text{ HT}$ and 9 mmol L^{-1} hydroquinone at a scan rate of 100 mV s^{-1} .

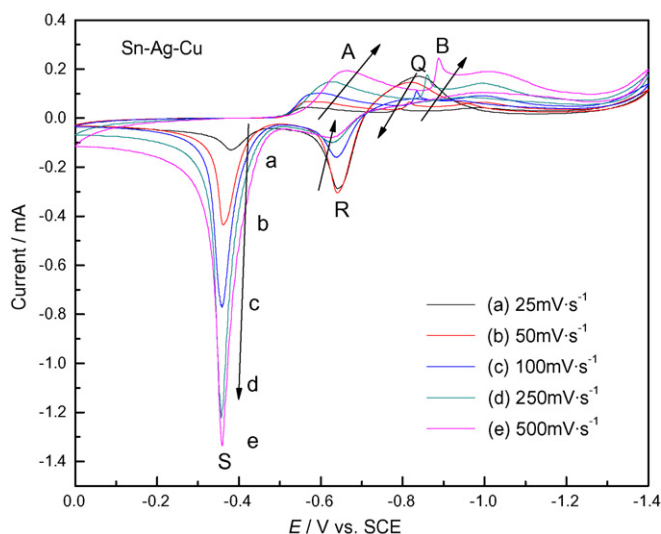


Fig. 13. CV curves of Sn–Ag–Cu alloy electrodeposited from a weakly acidic bath containing $0.20 \text{ mol L}^{-1} \text{ Sn}(\text{CH}_3\text{SO}_3)_2$, $4.5 \text{ mmol L}^{-1} \text{ AgI}$, $1.5 \text{ mmol L}^{-1} \text{ Cu}(\text{CH}_3\text{SO}_3)_2$, $0.60 \text{ mol L}^{-1} \text{ K}_4\text{P}_2\text{O}_7$, $1.35 \text{ mol L}^{-1} \text{ KI}$, $0.225 \text{ mol L}^{-1} \text{ TEA}$, $6.4 \text{ mmol L}^{-1} \text{ HT}$, 9 mmol L^{-1} hydroquinone at various scan rates of: (a) 25 mV s^{-1} , (b) 50 mV s^{-1} , (c) 100 mV s^{-1} , (d) 250 mV s^{-1} and (e) 500 mV s^{-1} .

F is the Faraday constant and α is the charge transfer coefficient [14].

As shown in Eq. (1), there is a linear relationship between I_p and $\nu^{1/2}$. As shown in Fig. 13, peak 'A' and peak 'B' are the co-deposit peaks of Sn–Ag–Cu alloy. Moreover, Fig. 14 indicates that the co-deposition of Sn–Ag–Cu alloy is an irreversible diffusion controlled process [15].

CA is an electrochemical technique commonly used to study the mechanism responsible for the electrodeposition of metals and alloys. During CA experiments, current–time transients are recorded as the potential is stepped from the open-circuit potential (OCP) to the potential at which the electrodeposition of metals or alloys would occur [16,17]. The Scharifker–Hills model shows two limiting nucleus growth mechanisms, one instantaneous nucleus growth mechanism and one progressive nucleus growth mechanism [18]. The theoretical transients of the instantaneous and the progressive nucleus growth, with three-dimensions (3D) under dif-

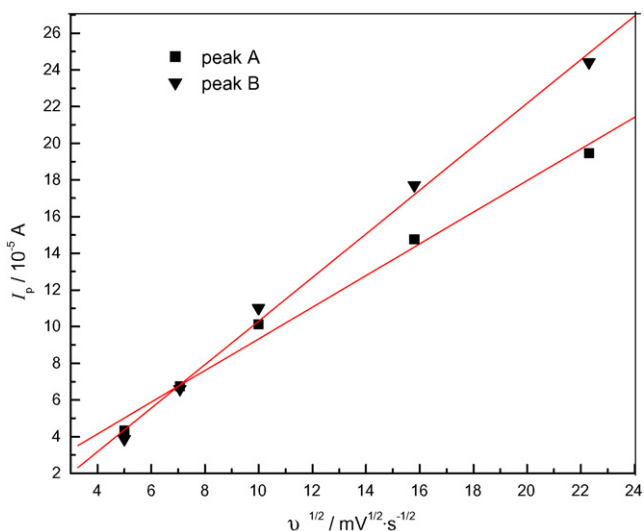


Fig. 14. The linear relationship between I_p and $\nu^{1/2}$, constructed from peak A (■) and peak B (▼), of curves shown in Fig. 13.

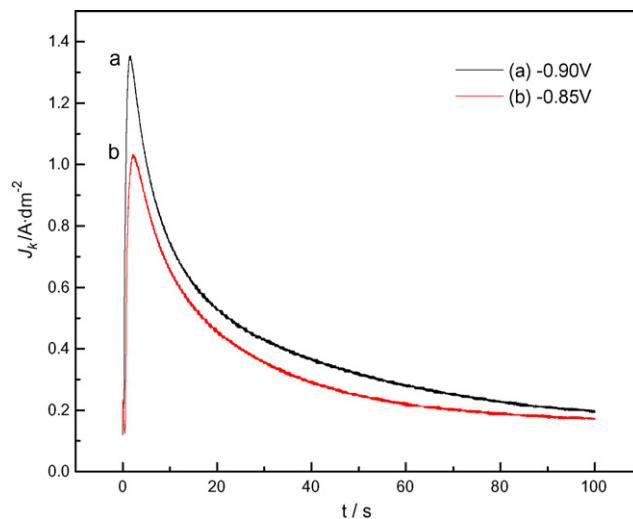


Fig. 15. Potentiostatic current transients of a Sn–Ag–Cu alloy electrodeposited from a weakly acidic bath containing $0.20 \text{ mol L}^{-1} \text{ Sn}(\text{CH}_3\text{SO}_3)_2$, $4.5 \text{ mmol L}^{-1} \text{ AgI}$, $1.5 \text{ mmol L}^{-1} \text{ Cu}(\text{CH}_3\text{SO}_3)_2$, $0.60 \text{ mol L}^{-1} \text{ K}_4\text{P}_2\text{O}_7$, $1.35 \text{ mol L}^{-1} \text{ KI}$, $0.225 \text{ mol L}^{-1} \text{ TEA}$, $6.4 \text{ mmol L}^{-1} \text{ HT}$ and 9 mmol L^{-1} hydroquinone at an applied potential from -0.40 V (OCP) to (a) -0.90 V and (b) -0.85 V vs. SCE.

fusion control, are given by:

$$\left(\frac{I}{I_m}\right)^2 = 1.9542 \left(\frac{t}{t_m}\right)^{-1} \left\{ 1 - \exp \left[-1.2564 \left(\frac{t}{t_m}\right) \right] \right\}^2 \quad (2)$$

$$\left(\frac{I}{I_m}\right)^2 = 1.2254 \left(\frac{t}{t_m}\right)^{-1} \left\{ 1 - \exp \left[-2.3367 \left(\frac{t}{t_m}\right)^2 \right] \right\}^2 \quad (3)$$

where I and t are the current density and time, respectively, and I_m and t_m are the maximum values of the current transients.

As shown in Fig. 13, the maximum potential of peak 'B' is between -0.85 V and -0.90 V . As discussed earlier, the electrodeposition of Sn–Ag–Cu alloy in the above potential range occurs under diffusion control. Therefore, during the CA experiments, the potentials were stepped from -0.4 V (OCP) to -0.90 V and -0.85 V , respectively. The current–time transients are as shown in Fig. 15. The sudden change in the value of the current in these curves is attributed to the double layer charge. However, a typical response of nucleation and growth occurs immediately after that. By using the Scharifker–Hills model, the corresponding data were calculated as shown in Fig. 16. Fig. 16 shows that the actual nucleus growth curves, of Sn–Ag–Cu alloy on the surface of GCE, are between theoretical instantaneous and progressive nucleation curves. Wu et al. [19] found that the nucleation mechanism of Zn on the surface of GCE is 3D progressive in the solutions that contained additives. The adsorption of additives would result in a decreasing number of the metal adatoms at a given overpotential. In this case, HT is an additive that can adsorb on the surface of electrode, increase cathodic polarization, inhibit the formation of nucleus, and possibly cause progressive nucleation of the Sn–Ag–Cu alloy. Palomar-Pardavé et al. [20] found that the experimental values of current will be consistently higher than the theoretical instantaneous current; particularly when $t > t_m$ in the presence of protons reduction reaction occurring simultaneously with Co electrodeposition. The average cathodic current efficiency for the electrodeposition process of Sn–Ag–Cu alloy is about 30%. This is attributed to the vigorous hydrogen evolution that occurs simultaneously with the nucleation [11], and can lead to the increase of experimental currents. Therefore, considering the presence of additives and the hydrogen evolution, we believe that the actual nucleus growth mechanism of the Sn–Ag–Cu alloy is represented by the progressive nucleation model.

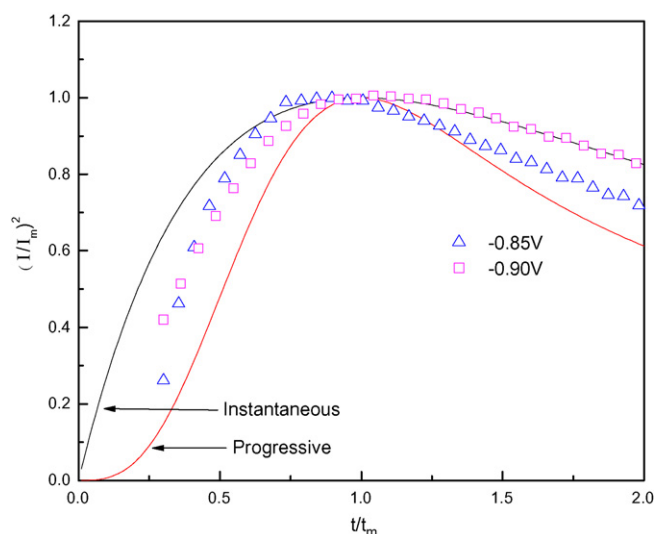


Fig. 16. Nondimensional plots of $(I/I_m)^2 - t/t_m$ for the current transients of a Sn–Ag–Cu alloy electrodeposited from a weakly acidic bath containing 0.20 mol L^{-1} $\text{Sn}(\text{CH}_3\text{SO}_3)_2$, 4.5 mmol L^{-1} AgI, 1.5 mmol L^{-1} $\text{Cu}(\text{CH}_3\text{SO}_3)_2$, 0.60 mol L^{-1} $\text{K}_4\text{P}_2\text{O}_7$, 1.35 mol L^{-1} KI, 0.225 mol L^{-1} TEA, 6.4 mmol L^{-1} HT and 9 mmol L^{-1} hydroquinone at an applied potential from -0.40 V (OCP) to (Δ) -0.85 V and (\square) -0.90 V vs. SCE.

4. Conclusions

The electrodeposition behavior and nucleus growth mechanism of Sn–Ag–Cu alloy deposited from bath containing 0.20 mol L^{-1} $\text{Sn}(\text{CH}_3\text{SO}_3)_2$, 4.5 mmol L^{-1} AgI, 1.5 mmol L^{-1} $\text{Cu}(\text{CH}_3\text{SO}_3)_2$, 0.60 mol L^{-1} $\text{K}_4\text{P}_2\text{O}_7$, 1.35 mol L^{-1} KI, 0.225 mol L^{-1} TEA, 6.4 mmol L^{-1} HT and 9 mmol L^{-1} hydroquinone on GCE, were studied using CV and CA techniques. The results of the study are summarized as follows:

Two cathodic peaks at -0.6 V and -0.85 V in CV curves, during the forward scan towards the negative potentials, correspond to the irreversible deposition of a solid solution of tin, silver and copper. The UPD of Sn occurs at -0.6 V , during the cathodic period.

The quantity of Ag and Cu in the Sn–Ag–Cu alloy decreases for increasingly negative values of cathodic potential. During the forward scan, towards the positive potentials of CV testing, cathodic peaks at -0.85 V correspond to the reduction of transient complex ions $[\text{Sn}(\text{TEA})_x]^{2+}$ on the surface of the cathode. The formation and reduction of $[\text{Sn}(\text{TEA})_x]^{2+}$ is a diffusion controlled process.

Considering the presence of additives and the hydrogen evolution, we believe that the actual nucleus growth mechanism of the Sn–Ag–Cu alloy on the surface of the GCE is represented by the progressive nucleation model.

Acknowledgment

This work was supported by the Science and Technology Commission Foundation of Harbin City (No. 2005AA5CG156).

References

- [1] H. Sonoda, K. Nakamura, WO Patent 2 004 011 698 (2004).
- [2] N. Kaneko, M. Komatsu, T. Kurashina, S. Arai, N. Shinohara, *Electrochemistry (Jpn.)* 73 (2005) 951.
- [3] B. Kim, T. Titzdorf, *J. Electrochem. Soc.* 150 (2003) C53.
- [4] K. Zeng, K.N. Tu, *Mater. Sci. Eng. R* 38 (2002) 55.
- [5] S. Joseph, G.J. Phatak, *Surf. Coat. Technol.* 202 (2008) 3023.
- [6] S. Miura, JP Patent 3 662 577 (2005).
- [7] M. Fukuda, K. Imayoshi, Y. Matsumoto, *Surf. Coat. Technol.* 169/170 (2003) 128.
- [8] P. Ozga, *Arch. Met. Mater.* 51 (2003) 413.
- [9] F. Guo, S. Choi, K.N. Subramanian, T.R. Bieler, J.P. Lucas, A. Achari, M. Paruchuri, *Mater. Sci. Eng. A* 351 (2003) 190.
- [10] I. Shohji, T. Yoshida, T. Takahashi, S. Hioki, *Mater. Sci. Eng. A* 366 (2004) 50.
- [11] J. Zhang, M. An, L. Chang, G. Liu, *Electrochim. Acta* 53 (2008) 2637.
- [12] A.E. Alvarez, D.R. Salinas, *J. Electroanal. Chem.* 566 (2004) 393.
- [13] M.C. Santos, L.O.S. Bulhões, *Electrochim. Acta* 48 (2003) 2607.
- [14] A.J. Bard, L.R. Faulkner, *Electrochemical Methods Fundamentals and Applications* (second version in Chinese), Chemical Industry Press, Beijing, 2005, p. 162.
- [15] Z. Chen, M.L. Zhang, W. Han, Z.Y. Hou, Y.D. Yan, *J. Alloy. Comp.* 464 (2008) 174.
- [16] M. Gu, *Electrochim. Acta* 52 (2007) 4443.
- [17] A.N. Correia, M.X. Façanha, P.L. Neto, *Surf. Coat. Technol.* 201 (2007) 7216.
- [18] B. Scharifker, G. Hills, *Electrochim. Acta* 28 (1983) 878.
- [19] H.H. Wu, S.K. Xu, S.M. Zhou, *Acta Physico-Chim. Sin. (Chn.)* 1 (1985) 357.
- [20] M. Palomar-Pardavé, B.R. Scharifker, E.M. Arce, M. Romero-Romo, *Electrochim. Acta* 50 (2005) 4736.